Electronic Supporting Information

Triazine Pyridinium Derivative Cascade Assembly Extended FRET for Two-Photon NIR Targeted Cells Imaging

*Xuan Zhao, Xiaolu Zhou, Wen-Wen Xing and Yu Liu**

College of Chemistry, State Key Laboratory of Elemento-Organic Chemistry, Nankai University, Tianjin 300071, P. R. China

* E-mail: yuliu@nankai.edu.cn

Table of Contents

Section I. Materials and Measurements

Materials. All reagents and solvents were purchased from commercial suppliers and used without purification unless specified otherwise. Ultrapure water was obtained after passing through a water ultra-purification system.

Measurements. ^{1}H NMR and ^{13}C NMR spectra were recorded on a Bruker DMX 400 MHz spectrometer at room temperature. High-resolution mass spectra (HRMS) were measured on 6520 Q-TOF LC/MS (Agilent). UV-vis spectra were recorded in a quartz cell (light path = 1 cm) on a Thermo Fisher Scientific EVO300 PC spectrophotometer with a PTC-348WI temperature controller. Fluorescence emission spectra were recorded on a JASCO FP-750 spectrometer in a conventional quartz cell (10 × 10 × 45 mm) at 298 K. Transmission electron microscopy (TEM) experiments were accomplished on FEI Tecnai G2 F20 under 200 KV and scanning electron microscopy (SEM) experiments were carried out on MERLIN Compact instrument. Zeta potentials and DLSs were measured by Brookhaven instrument (BI-200SM) equipped with a digital correlator (Turbo Corr.) at a scattering angle of 90°. Absolute fluorescence quantum yields and lifetime were carried out on a FLS980 instrument (Edinburg Instruments Ltd., Livingstone, UK).

Cell culture. Human cervical carcinoma cells (HeLa cells), Human lung adenocarcinoma cells (A549 cells) and the human embryonic kidney cells (293T cells) were all obtained from the Cell Resource Center, Chinese Academy of Medical Science Beijing. HeLa cancer cells and 293T normal cells were incubated with DMEM high glucose nutrient medium containing 10 % FBS and 1 % penicillin/ streptomycin and A549 cancer cells were cultured with Ham's F12 nutrient medium supplemented with 10 % FBS and 1 % penicillin/streptomycin.

Colocalization imaging. Cell images were captured on the Leika S8 microscope and

Olympus FV1000 Laser scanning confocal microscope. The well-cultured cells were incubated with HA-SC4AD-TAZpy-CB[7] ([HA] = 10 μg/mL, [SC4AD] = [TAZpy] = 2×10^{-5} M, [CB[7]] = 6×10^{-5} M, λ_{ex} = 370 nm) in a humidified incubator with 5 % CO_2 atmosphere at 37 °C for 12 h. Then, the cells were washed with PBS and stained with Mito-Tracker Red (100 nm, Sigma) at 310 K for 30 min. The cells were further washed three times with phosphate buffer solution, fixed with 4% paraformaldehyde for 15 min, and then observed with a confocal microscope. The cells were subjected to observation by an Olympus FV1000 fluorescence microscope immediately. The intracellular distribution of the HA-SC4AD-TAZpy-CB[7]: RhB: NiB light capturing system was investigated by the two-photon and confocal laser scanning microscopy under other conditions being consistent.

Cytotoxicity experiments. Hela and A549 cancer cells and 293T normal cells were plated at 96-well plates at a density of 5×10^4 cells per well in 100 μL corresponding cell culture medium for 24 h at 37 ℃ in 5 % CO_2. Next, the cells were treated with HA-SC4AD-TAZpy-CB[7] assembly for 12 h. The culture medium was discarded and the cells were washed with 0.01 M PBS twice at least. Then CCK8 solution was added to each well and then the cells were further incubated at 37 ºC for 1 h. The absorbance value was obtained by a microplate reader at 450 nm wavelength. Three replicates of each experiment were performed, and values herein stand for means ± standard deviations (SD).

Calculation of energy-transfer efficiency (Φ_{ET}). Energy transfer efficiency (Φ_{ET}), the fraction of the absorbed energy that is transferred to the acceptor is experimentally measured as a ratio of the fluorescence intensities of the donor in the absence and presence of the acceptor (I_D and I_{DA}). The energy transfer efficiency (Φ_{ET}) was calculated in aqueous solution.

$$\Phi_{ET} = 1 - I_{DA}/I_D$$

Section II. Synthetic Route of Compounds

TAZpy: TAZpy was synthesized according to the reported procedure. 4-hydroxybenzaldehyde (1.22 g, 10 mmol) and NaOH (0.4 g, 10 mmol) aqueous solution were added to the acetone solution (5 mL) of cyanuric chloride (0.46 g, 2.5 mmol). The mixture was stirred at room temperature for 24 h. After the reaction mixture was filtered, the white solid (**TAZ**) was washed with 10 % sodium hydroxide solution (3 × 25 mL) and double distilled water (2 × 25 mL) and then dried in vacuo (Yield: 85 %).[1] **TAZ**: ^{1}H NMR (400 MHz, $CDCl_3$, 298 K) δ: 10.00 (s, 3H), 7.92 (d, J = 8.4 Hz, 6H) 7.32 (d, J = 8.4 Hz, 6H). TAZ (0.44, 1.00 mmol) and 1-ethyl-4-methylpyridinium bromide 1 (0.76 g, 3.75 mmol) were dissolved in 30 mL ethanol and added a drop of piperidine into it, then refluxing for 12 hours. The solution was s concentrated and cooled to obtain a precipitate, which was filtered and washed with acetone and then dissolved in ethanol for recrystallization. The formed precipitate (**TAZpy**) was washed by acetone, and dried in vacuo, to give a yellow powder (Yield: 34 %). **TAZpy**: ^{1}H NMR (400 MHz, D_2O, 298 K) δ: 8.48 (d, J = 4.4 Hz, 6H), 7.83 (d, J = 3.8 Hz, 6H), 7.64-7.44 (m, 9H), 7.01 (dd, J = 15.9, 11.5 Hz, 3H), 6.85 (t, J = 9.3 Hz, 6H), 4.43 (m, J = 14.4, 7.4 Hz, 6H), 1.56 (t, J = 12.4 Hz, 9H). ^{13}C NMR (100 MHz, D_2O, 298 K) δ: 159.79, 155.52, 144.46,

142.29, 132.11, 129.30, 125.32, 122.04, 117.76, 57.65, 17.28. HR-ESI-MS: m/z calculated for $C_{48}H_{45}N_6O_3^{3+}$: $[TAZpy\text{-}3Br]^{3+}$, 251.1179; found, 251.1176.
SC4AD: **SC4AD** was prepared according to the literature.[2]

Section III. Characterization Data and Supplementary Instruction

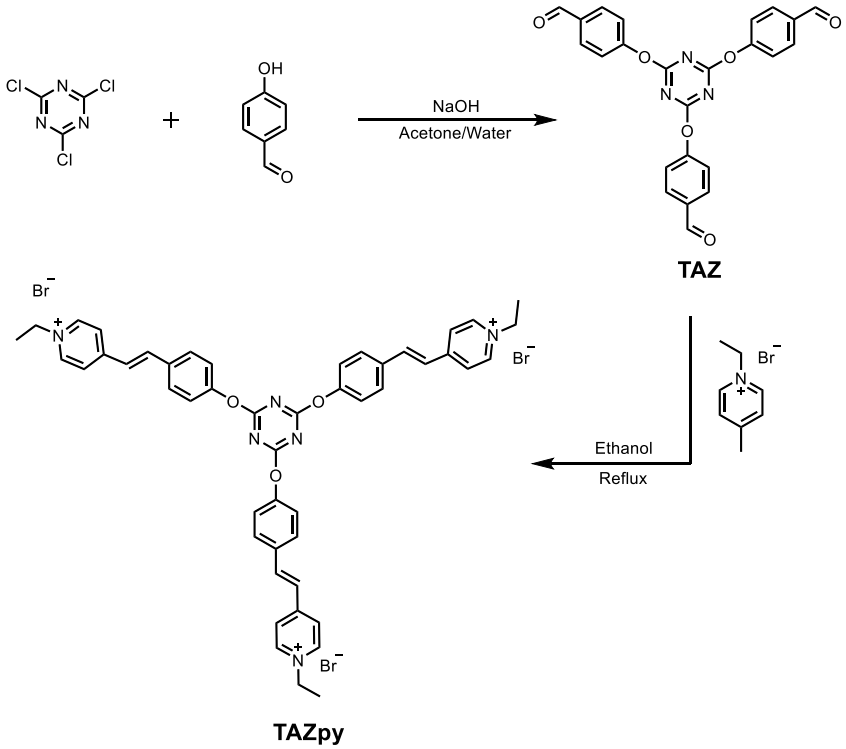

Scheme S1. Synthetic routes of **TAZ** and **TAZpy**.

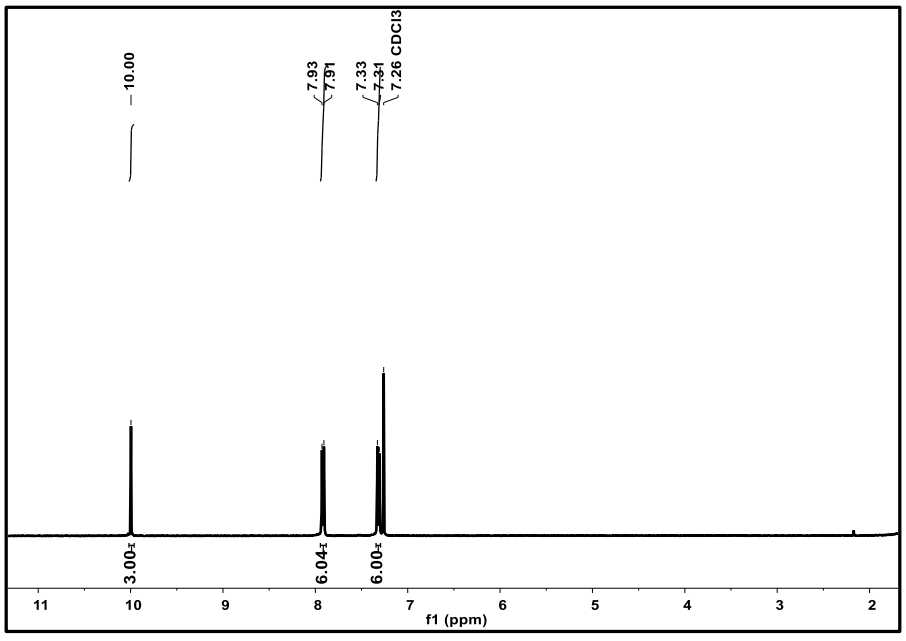

Fig, S1 ^{1}H NMR spectrum (400 MHz, $CDCl_3$, 298 K) of **TAZ**.

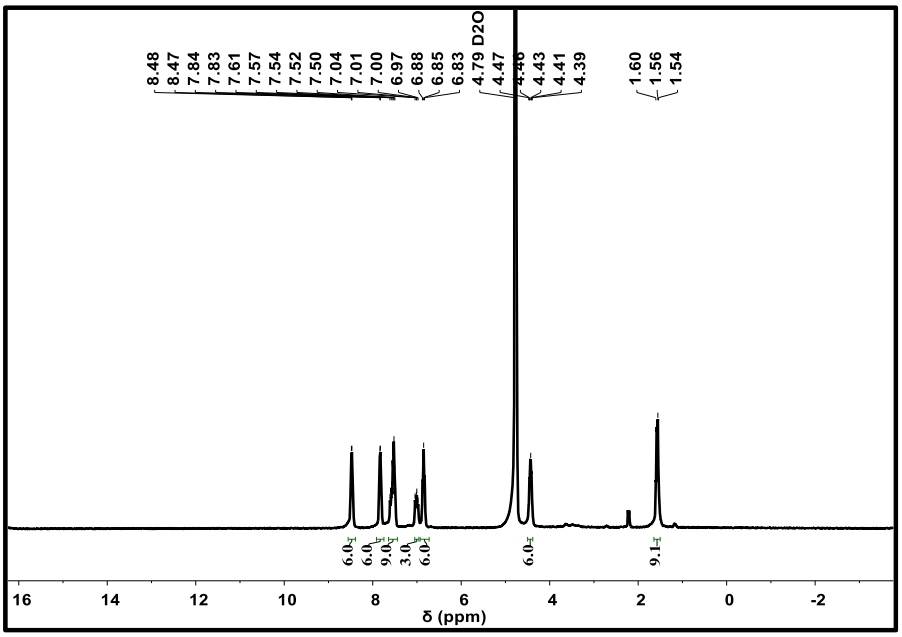

Fig. S2 ^{1}H NMR spectrum (400 MHz, DO_2, 298 K) of **TAZpy**.

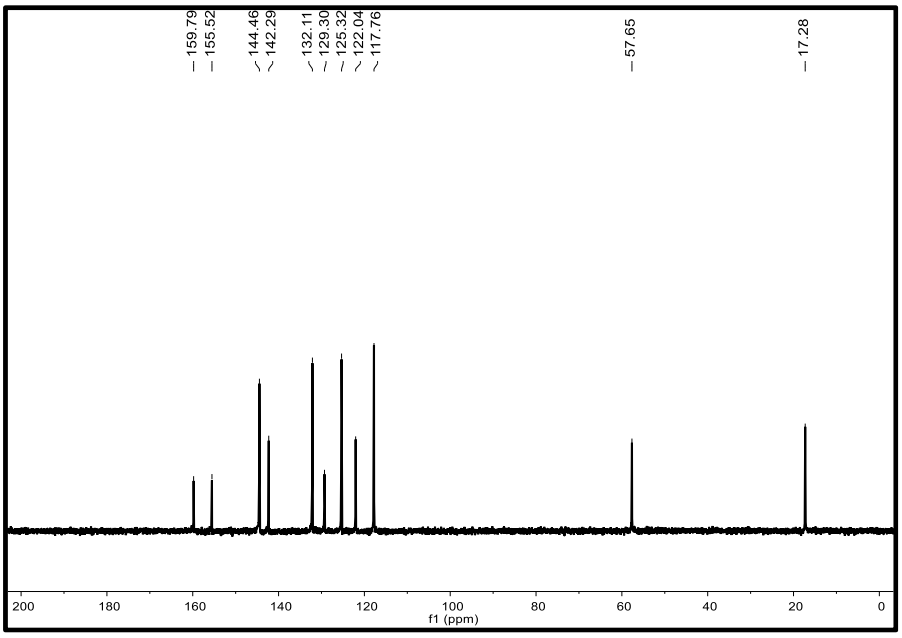

Fig. S3 ^{13}C NMR spectrum (100 MHz, DO_2, 298 K) of **TAZpy**.

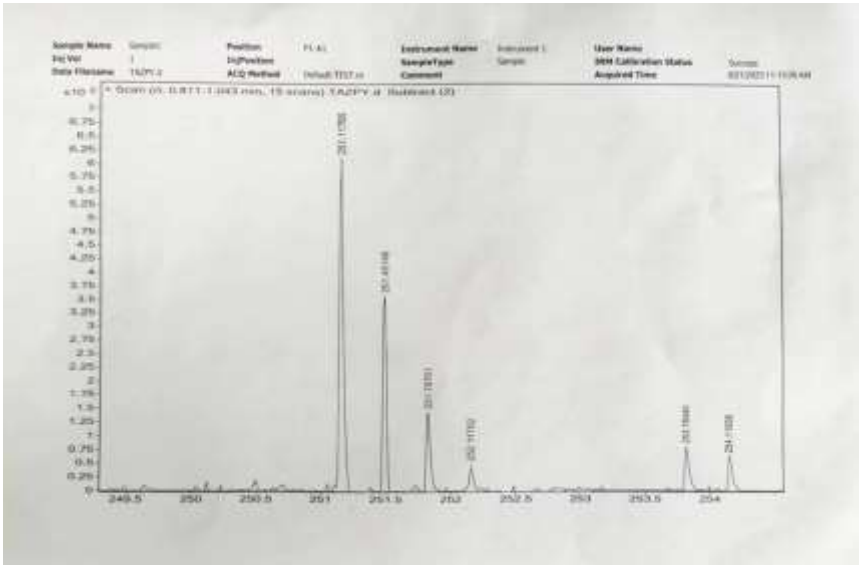

Fig. S4 HR-MS spectrum of **TAZpy**.

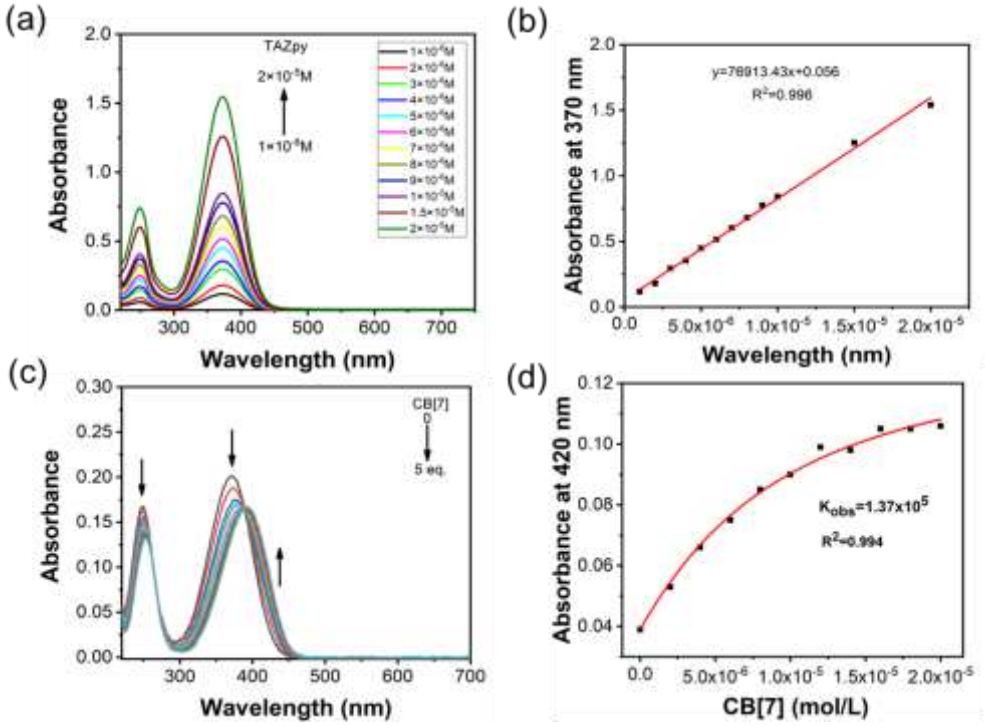

Fig. S5 (a) UV-vis absorbance spectra of TAZpy at different concentrations in aqueous solution; (b) Standard curve of TAZpy with absorption at 370 nm at different concentrations; (c) UV-vis Spectral changes of TAZpy (2×10^{-6} M) upon gradual addition of CB[7] ranging from 0 to 1×10^{-5} M in aqueous solution at 298 K; (d) The nonlinear curve fitting of the variation of UV-vis absorbance at 420 nm with the concentration of CB[7] to calculate the association constant.

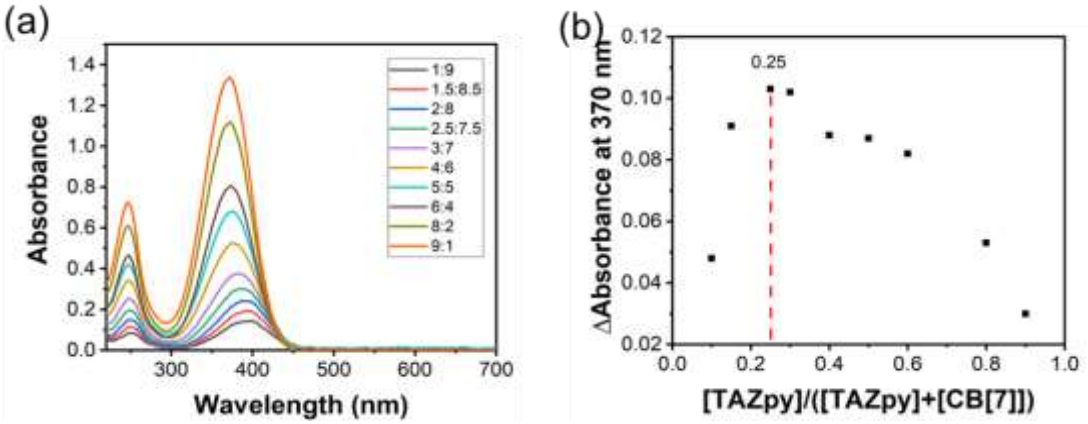

Fig. S6 (a) Absorption spectra of TAZpy in the presence of different ratios of CB[7] at 298 K; (b) Job plot of TAZpy complexation with CB[7] in aqueous solution at 298 K. Absorbance intensity changes of TAZpy recorded at 370 nm was used to analyze the binding ratio. The total concentration of guest and host is constant ([TAZpy] + [CB[7]] = 2×10^{-5} M).

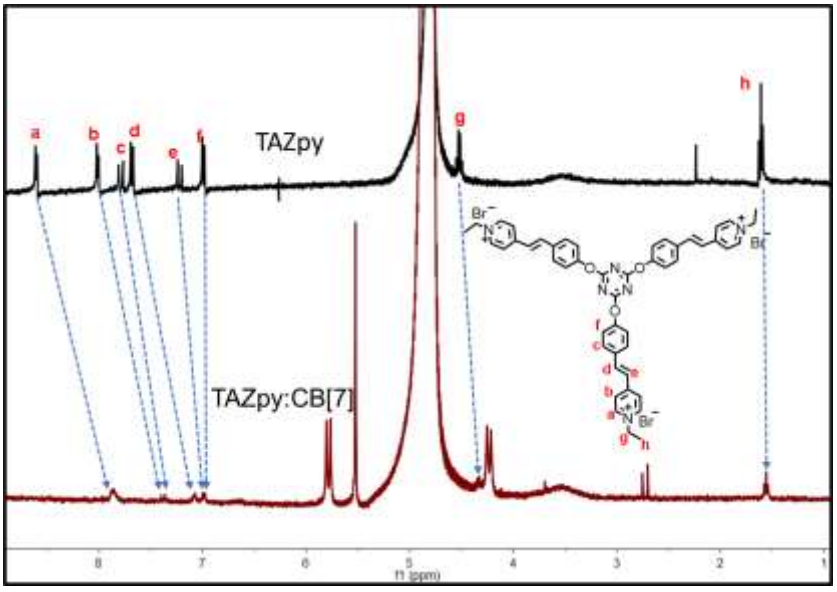

Fig. S7 ^{1}H NMR spectra (400 MHz, D_2O, 298 K) of TAZpy and TAZpy-CB[7] ([TAZpy] = 2×10^{-5} M, [CB[7]] = 6×10^{-5} M, TAZpy : CB[7] = 1:3).

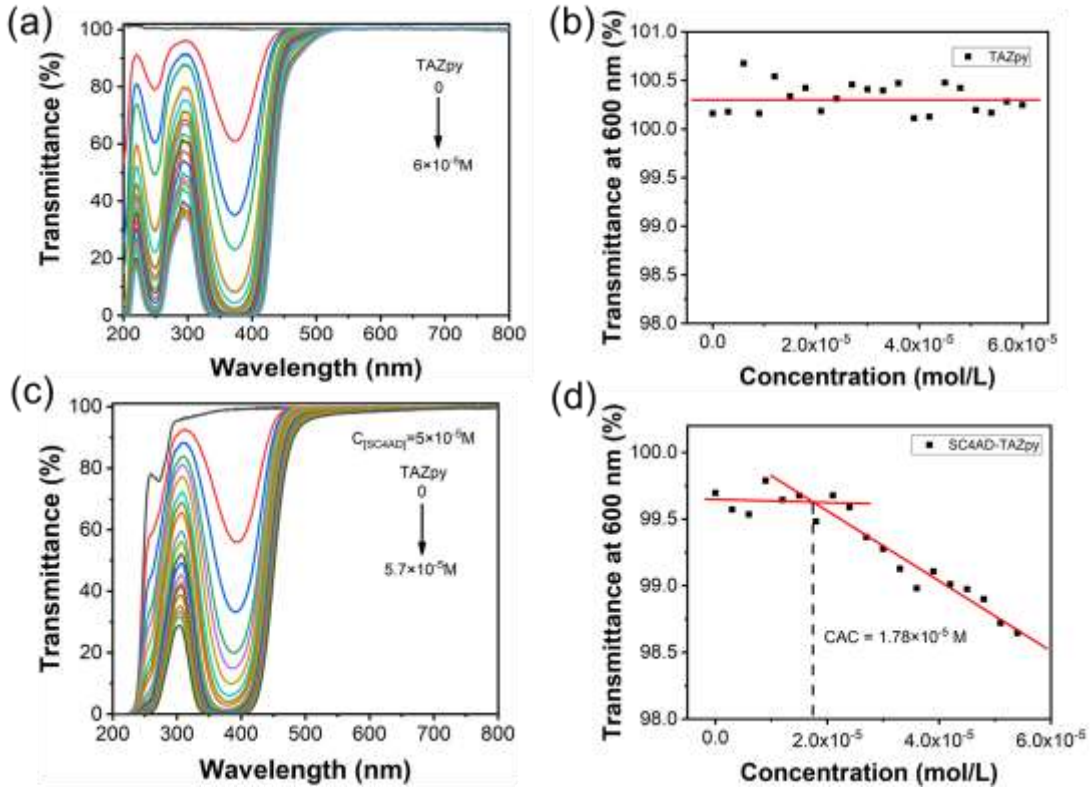

Fig. S8 (a) Optical transmittance of TAZpy at different concentrations in aqueous solution at 298 K; (b) Dependence of the optical transmittance at 600 nm at different concentrations of TAZpy; (c) Optical transmittance of SC4AD (5×10^{-5} M) with TAZpy at different concentrations in aqueous solution at 298 K; (d) Dependence of the optical transmittance at 600 nm on the TAZpy concentration in the presence of SC4AD (5×10^{-5} M) in aqueous solution at 298 K.

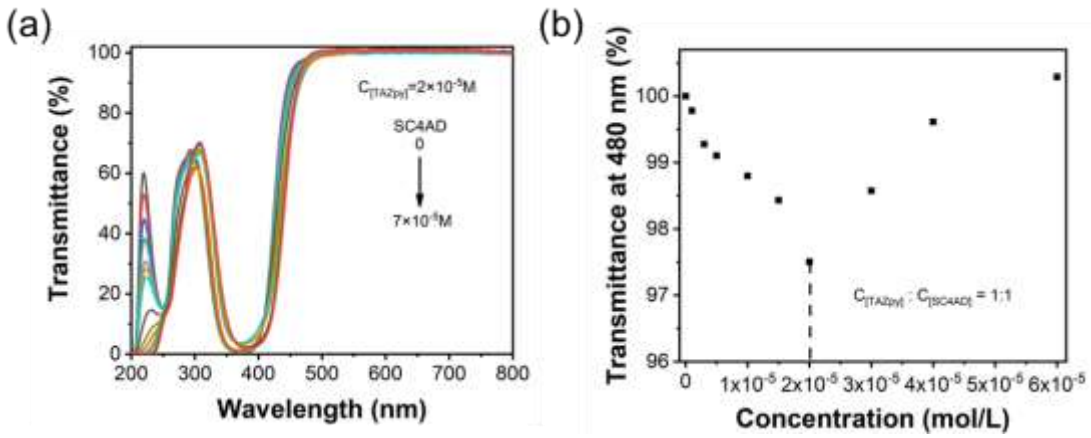

Fig. S9 (a) Optical transmittance of TAZpy (2×10^{-5} M) with SC4AD at different concentrations in aqueous solution at 298 K; (b) Dependence of the optical transmittance at 480 nm on the SC4AD concentration with a fixed TAZpy concentration (2×10^{-5} M) in aqueous solution at 298 K.

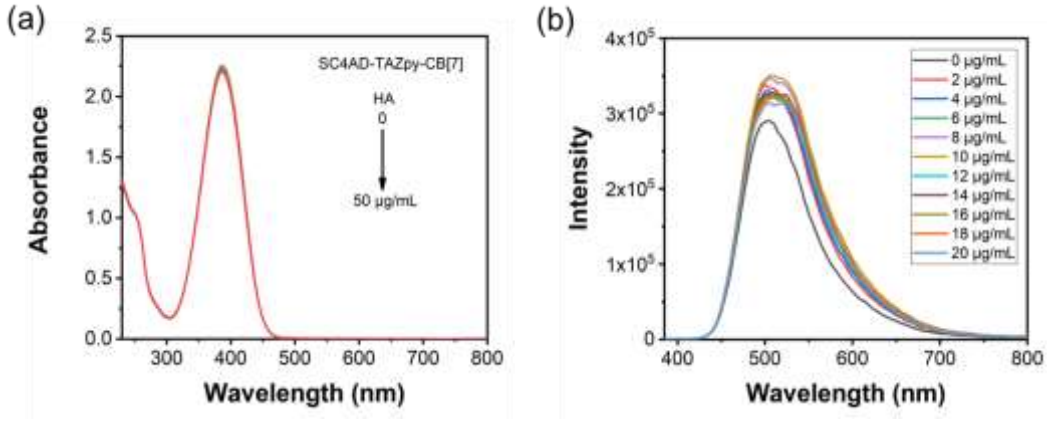

Fig. S10 (a) UV-vis absorbance spectra and (b) Fluorescence spectra of SC4AD-TAZpy-CB[7] with HA at different concentrations in aqueous solution at 298 K ([SC4AD] = [TAZpy] = 2×10^{-5} M, [CB[7]] = 6×10^{-5} M, λ_{ex} = 370 nm).

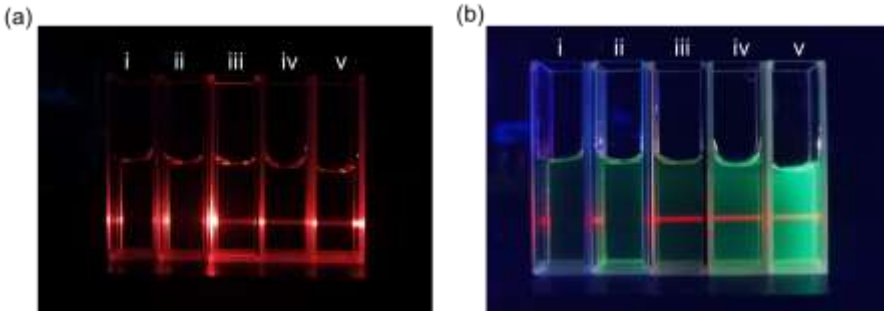

Fig. S11 Tyndall effects of TAZpy (i), TAZpy-CB[7] (ii), SC4AD-TAZpy (iii), SC4AD-TAZpy-CB[7] (iv) and HA-SC4AD-TAZpy-CB[7] (v) in the dark (a) and at 365nm light irradiation (b).

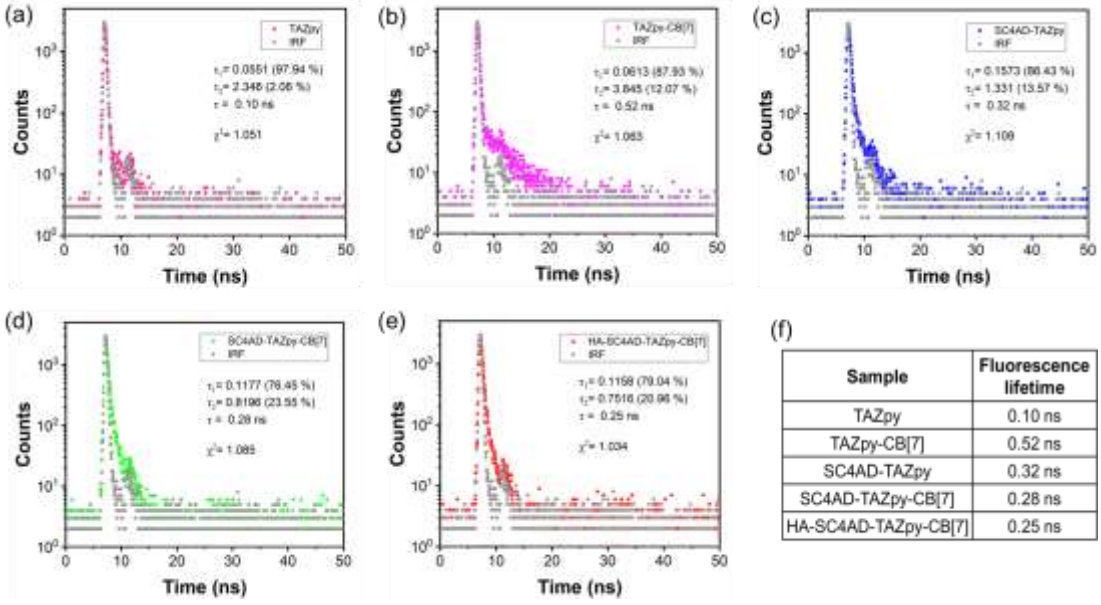

Sample	Fluorescence lifetime
TAZpy	0.10 ns
TAZpy-CB[7]	0.52 ns
SC4AD-TAZpy	0.32 ns
SC4AD-TAZpy-CB[7]	0.28 ns
HA-SC4AD-TAZpy-CB[7]	0.25 ns

Fig. S12 The time-resolved fluorescence decay curve of (a) TAZpy, (b) TAZpy-CB[7], (c) SC4AD-TAZpy, (d) SC4AD-TAZpy-CB[7] and (e) HA-SC4AD-TAZpy-CB[7]; (f) Fluorescence lifetime of 5 samples.(λ_{ex} = 450 nm)

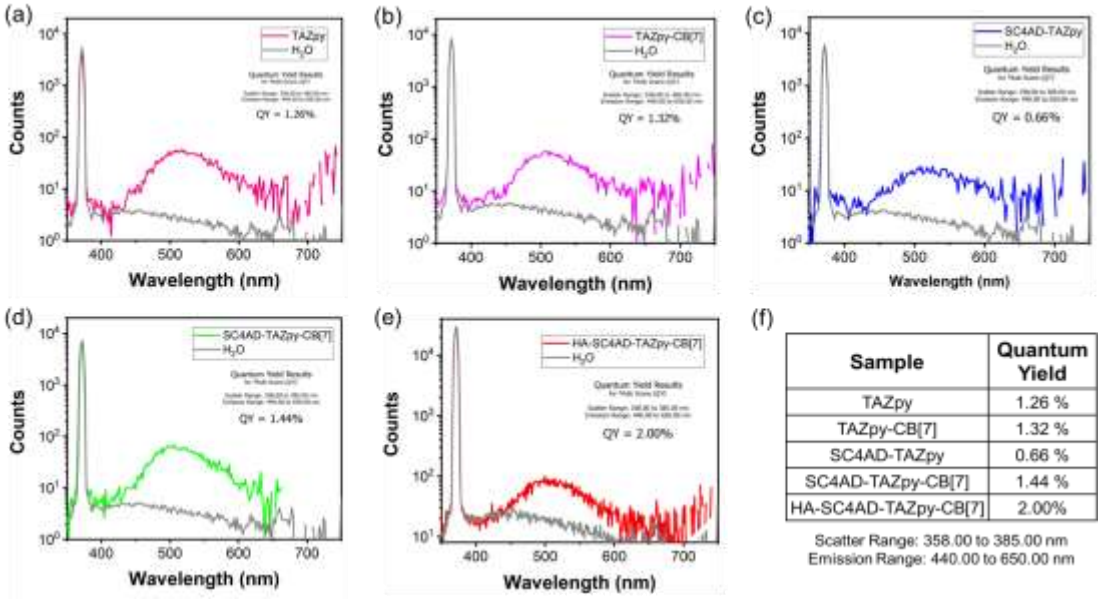

(f)

Sample	Quantum Yield
TAZpy	1.26 %
TAZpy-CB[7]	1.32 %
SC4AD-TAZpy	0.66 %
SC4AD-TAZpy-CB[7]	1.44 %
HA-SC4AD-TAZpy-CB[7]	2.00%

Scatter Range: 358.00 to 385.00 nm
Emission Range: 440.00 to 650.00 nm

Fig. S13 The quantum yield of (a) TAZpy, (b) TAZpy-CB[7], (c) SC4AD-TAZpy, (d) SC4AD-TAZpy-CB[7] and (e) HA-SC4AD-TAZpy-CB[7]; (f) Fluorescence quantum efficiency of 5 samples. (λ_{ex} = 370 nm)

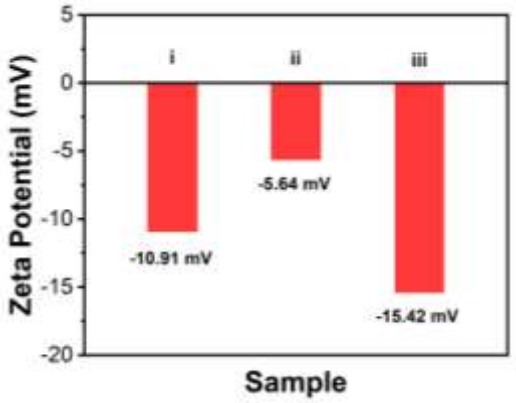

Fig. S14 Zeta potential of SC4AD-TAZpy (i), SC4AD-TAZpy-CB[7] (ii), HA-SC4AD-TAZpy-CB[7] (iii).

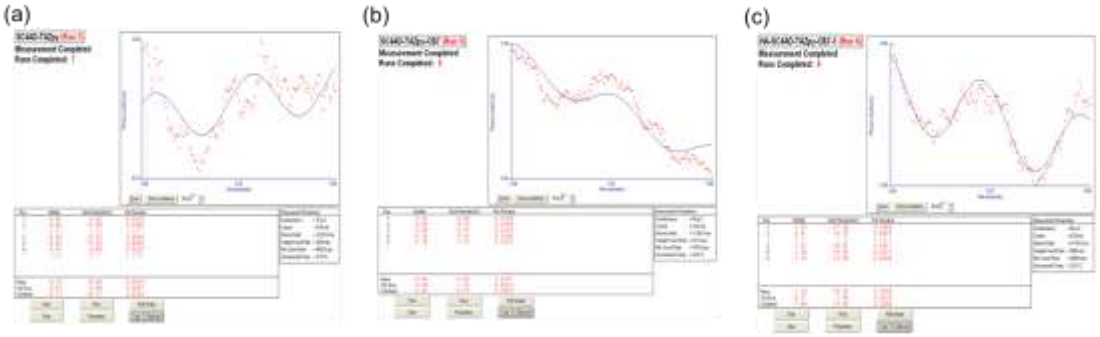

Fig. S15 The original data of Zeta potential of (a) SC4AD-TAZpy, (b) SC4AD-TAZpy-CB[7] and (c) HA-SC4AD-TAZpy-CB[7] ([HA] = 10 μg/mL, [SC4AD] = [TAZpy] = 2×10^{-5} M, [CB[7]] = 6×10^{-5} M).

The zeta potential of SC4AD-TAZpy, SC4AD-TAZpy-CB[7] and HA-SC4AD-

TAZpy-CB[7] were measured and calculated as -10.91 mV, -5.64 mV and -15.42 mV, respectively.

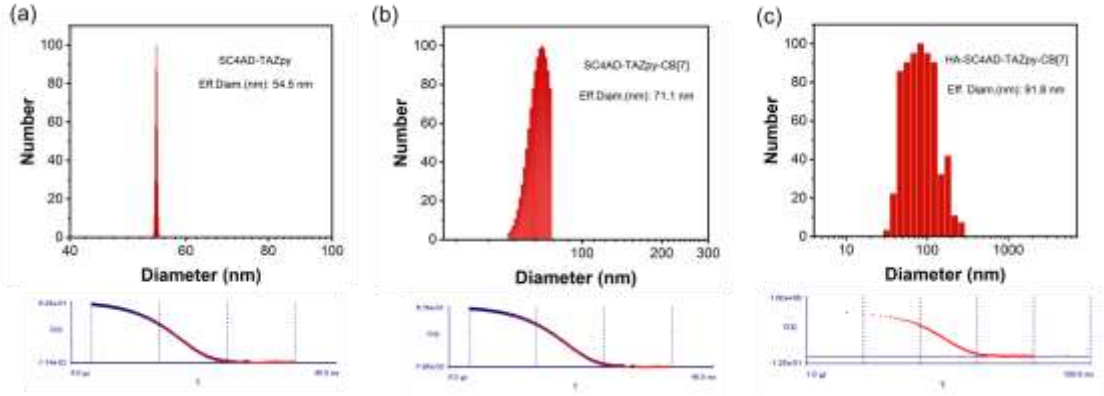

Fig. S16 DLS data of (a) SC4AD-TAZpy, (b) SC4AD-TAZpy-CB[7] and (c) HA-SC4AD-TAZpy-CB[7] ([HA] = 10 μg/mL, [SC4AD] = [TAZpy] = 2×10^{-5} M, [CB[7]] = 6×10^{-5} M).

DLS was used to measure the average effective diameter nanoparticles in aqueous solutions. DLS data revealed that the average particle sizes of the SC4AD-TAZpy, SC4AD-TAZpy-CB[7] and HA-SC4AD-TAZpy-CB[7] were about 54.5 nm, 71.1 nm and 91.8 nm severally, which proved the formation of abundant and stable supramolecular assemblies.

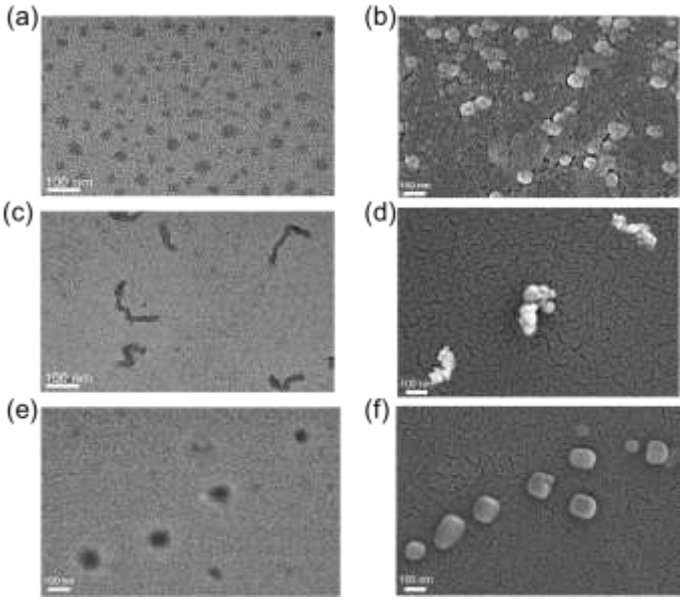

Fig. S17 (a) TEM image and (b) SEM image of SC4AD-TAZpy; (c) TEM image and (d) SEM image of SC4AD-TAZpy-CB[7]; (e) TEM image and (f) SEM image of HA-SC4AD-TAZpy-CB[7].

SC4AD-TAZpy gave obvious spherical nanoparticles with the diameters about 50 nm. In contrast, the SC4AD-TAZpy-CB[7] assembly existed as curved nanofibers with a uniform width of *ca.* 20 nm and a length of *ca.* 100 nm. The larger nanoparticles HA-SC4AD-TAZpy-CB[7] were obtained by adding HA in aqueous solution via the

electrostatic interaction, which possessed diameters around 100 nm. SEM images were consistent with the TEM results.

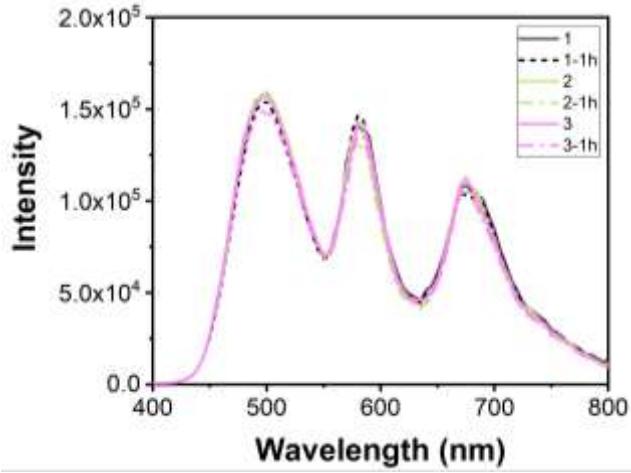

Fig. S18 Fluorescence spectra of three solutions of HA-SC4AD-TAZpy-CB[7]: RhB: NiB after 1h in darkness (3000:60:15, λ_{ex} = 370 nm).

Repeated experiments showed that the HA-SC4AD-TAZpy-CB[7]: RhB: NiB assembly was stable and repeatable.

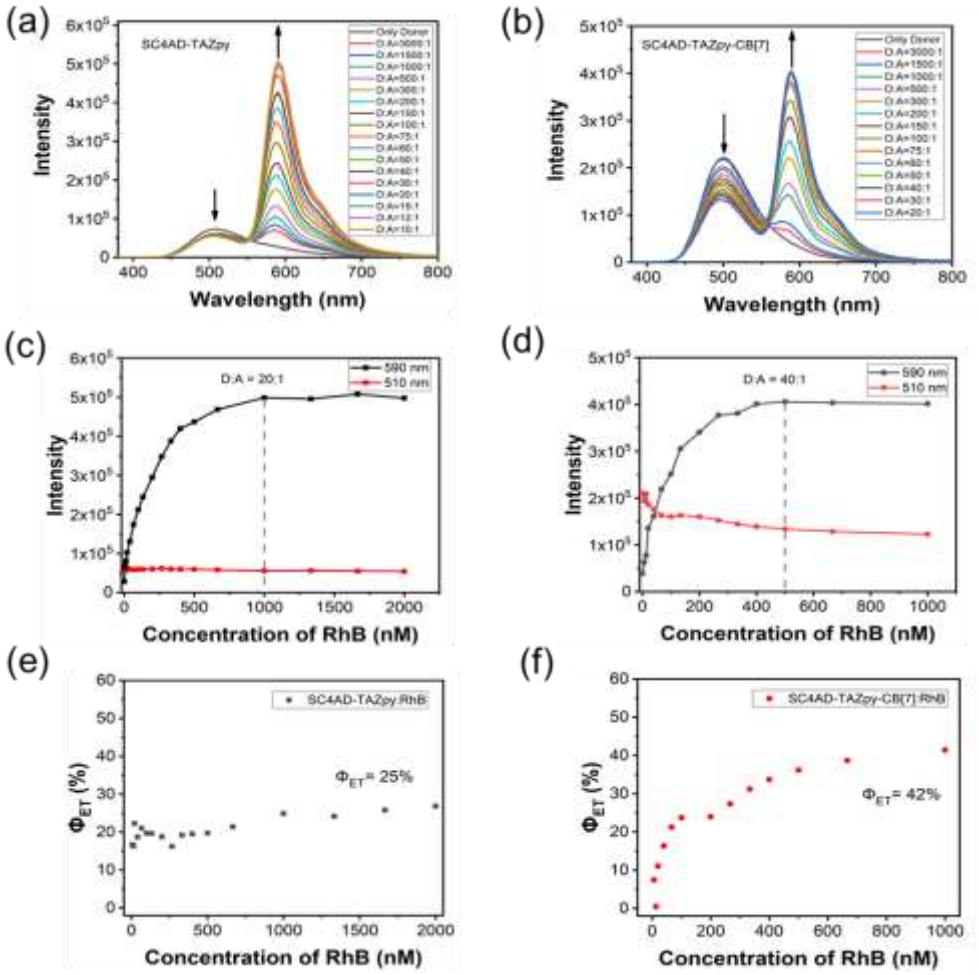

Fig. S19 (a) Fluorescence spectra of a) SC4AD-TAZpy:RhB and (b) SC4AD-TAZpy-

CB[7]:RhB at different donor/acceptor ratios; The changes of fluorescence intensity of (c) SC4AD-TAZpy:RhB and (d) SC4AD-TAZpy-CB[7]: RhB at 510 nm and at 590 nm; Φ_{ET1} of (e) SC4AD-TAZpy:RhB and (f) SC4AD-TAZpy-CB[7]: RhB at different donor/ acceptor ratios ([SC4AD] = [TAZpy] = 2×10^{-5} M, [CB[7]] = 6×10^{-5} M, λ_{ex} = 370 nm Slit/Slit: 2/2).

The fluorescence emission of SC4AD-TAZpy and SC4AD-TAZpy-CB[7] at 510 nm decreased, while the emission of acceptor I intensity at 590 nm was gradually enhanced with the increase of RhB. Φ_{ET1} (SC4AD-TAZpy: RhB) = 25 % (20:1), Φ_{ET1} (SC4AD-TAZpy-CB[7]: RhB) = 42 % (40:1).

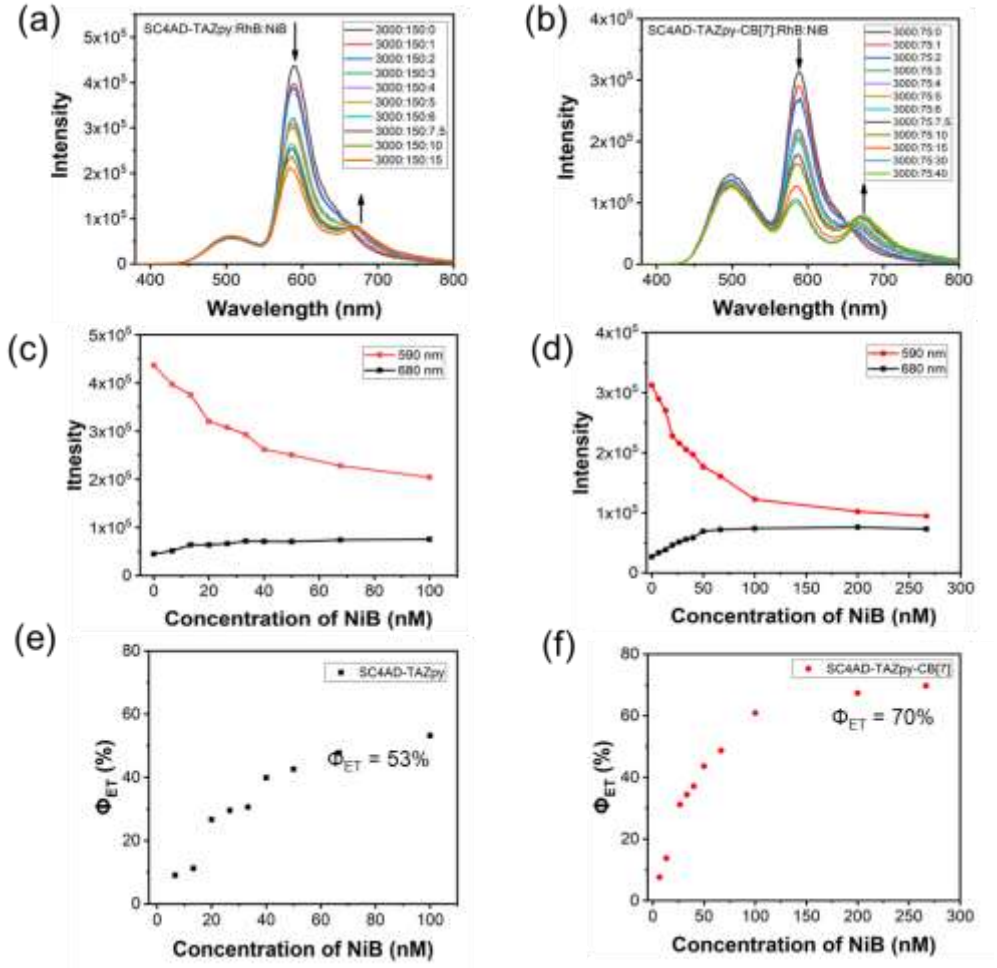

Fig. S20 Fluorescence spectra of (a) SC4AD-TAZpy:RhB:NiB and (b) SC4AD-TAZpy-CB[7]: RhB: NiB at different donor/acceptor ratios; The changes of fluorescence intensity of (c) SC4AD-TAZpy:RhB:NiB and d) SC4AD-TAZpy-CB[7]: RhB: NiB at 590 nm and at 680 nm; Φ_{ET2} of (e) SC4AD-TAZpy:RhB:NiB and (f) SC4AD-TAZpy-CB[7]: RhB: NiB at different donor/acceptor ratios ([SC4AD] = [TAZpy] = 2×10^{-5} M, [CB[7]] = 6×10^{-5} M, λ_{ex} = 370 nm Slit/Slit: 2/2).

The experimental phenomena were observed to be similar to the cascade FRET process for HA-SC4AD-TAZpy-CB[7]:RhB with the further addition of acceptor II

(NiB). The NIR emission of NiB kept enhanced along with continuous reduction of donor emission when gradually increasing the concentration of NiB. Φ_{ET2} (SC4AD-TAZpy: RhB: NiB) = 53 % (3000:150:15), Φ_{ET2} (SC4AD-TAZpy-CB[7]: RhB) = 70 % (3000:75:40).

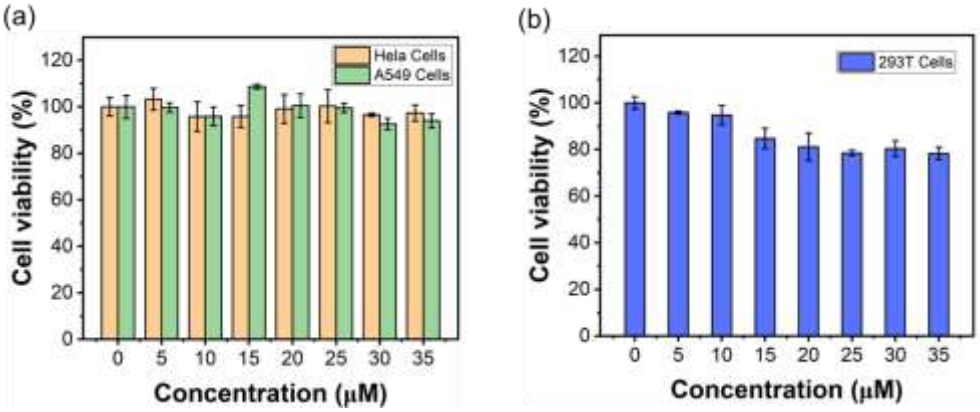

Fig. S21 Cell viability of (a) HeLa cancer cells and A549 cancer cells, and (b) 293T normal cells after 24 h incubation with different concentrations of HA-SC4AD-TAZpy-CB[7]. N=4 independent experiments, with the bar data indicating mean ± SD.

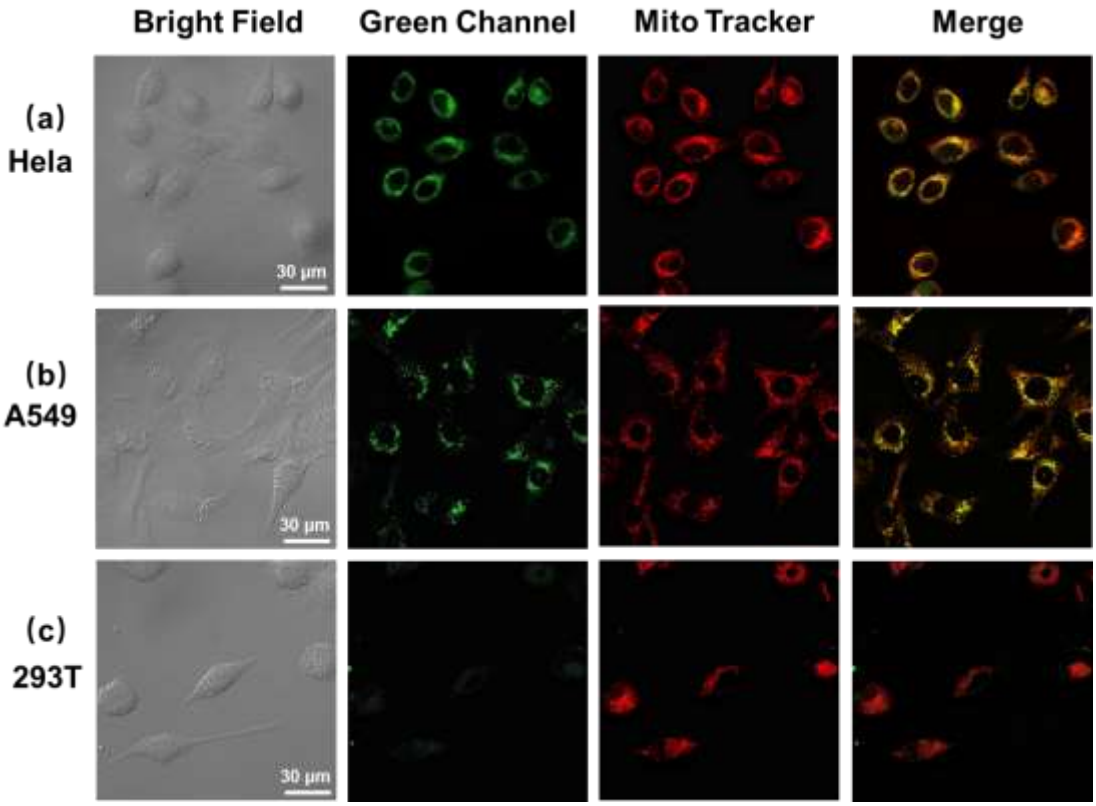

Fig. S22 Cellular co-localization imaging of (a) Hela cancer cells, (b) A549 cancer cells and (c) 293T normal cells after co-staining with the HA-SC4AD-TAZpy-CB[7] assembly and Mito-Tracker Red. HA-SC4AD-TAZpy-CB[7] was collected from 480 to 560 nm (λ_{ex} = 405 nm) and Mito-Tracker Red was collected from 590 to 690 nm (λ_{ex} = 570 nm).

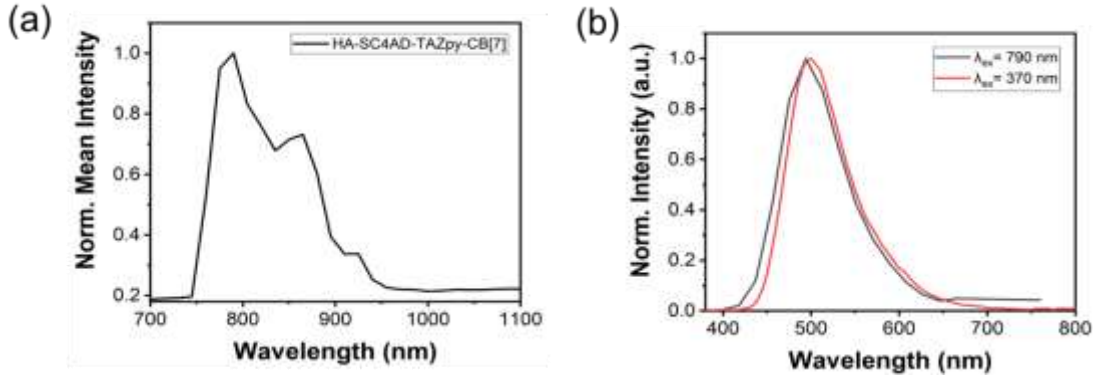

Fig. S23 (a) Two-photon excitation spectrum of HA-SC4AD-TAZpy-CB[7] in aqueous solution; (b) Emission spectra of supramolecular assembly HA-SC4AD-TAZpy-CB[7] excited at 370 nm and 790 nm.

Section IV. References

1. M. Afshari, M. Dinari, H. Farrokhpour, F. Zamora, *ACS Appl. Mater. Interfaces*, 2022, **14**, 22398.
2. K. P. Wang, Y. Chen, Y. Liu, *Chem. Commun.*, 2015, **51**, 1647.